International Journal of Nanomedicine

Dovepress

open access to scientific and medical research

Open Access Full Text Article

ORIGINAL RESEARCH

Subcellular Organelle-Targeted Nanostructured Lipid Carriers for the Treatment of Metastatic Breast Cancer

Wenli Dang[1–3], Bin Xing[1–3], Xintao Jia[1–3], Ying Zhang[1–3], Bei Jia[1–3], Changxiang Yu[1–3], Jiachen He[1–3], Ziwei Li[1–3], Huihui Li[1–3], Zhidong Liu[1–3]

[1]State Key Laboratory of Component-Based Chinese Medicine, Tianjin University of Traditional Chinese Medicine, Tianjin, People's Republic of China; [2]Engineering Research Center of Modern Chinese Medicine Discovery and Preparation Technique, Ministry of Education, Tianjin University of Traditional Chinese Medicine, Tianjin, People's Republic of China; [3]Haihe Laboratory of Modern Chinese Medicine, Tianjin, People's Republic of China

Correspondence: Zhidong Liu, Tianjin University of Traditional Chinese Medicine, No. 10 Poyang Lake Road, 301617, Tuanbo New Town, Jinghai District, Tianjin, People's Republic of China, Tel +86 22-59596170, Email lonerliuzd@163.com

Background: Subcellular organelle targeted nano-formulations for cancer treatment are receiving increasing attention owing to their benefits of precise drug delivery, maximized therapeutic index, and reduced off-target side effects. The nucleus and mitochondria, as the main subcellular organelles, are the significant organelles responsible for maintaining cell operation and metabolism. They can be involved in many essential physiological and pathological processes such as cell proliferation, organism metabolism, intracellular transportation, and play a critical role in regulating cell biology. Meanwhile, breast cancer metastasis is one of the leading causes of death in breast cancer patients. With the development of nanotechnology, nanomaterials have been widely used in tumor therapy.

Methods: We designed a subcellular organelle targeted nanostructured lipid carriers (NLC) to deliver paclitaxel (PTX) and gambogic acid (GA) to tumor tissues.

Results: Due to the surface of NLC being modified by subcellular organelle targeted peptide, the PTX and GA co-loaded NLC can accurately release PTX and GA in tumor cells. This property makes NLC able to easy to enter tumor site and target the specific subcellular organelle. The modified NLC can efficiently inhibit the growth of 4T1 primary tumor and lung metastasis, which may be related to the down-regulation of matrix metalloproteinase-9 (MMP-9) and BCL-2 levels, up-regulation of E-cadherin level, and antagonized PTX-induced increase of C-C chemokine ligand 2 (CCL-2) levels by GA. Meanwhile, the synergistic anti-tumor effect of GA and PTX has also been verified in vitro and in vivo experiments.

Conclusion: The subcellular organelle targeted peptide modified PTX+GA multifunctional nano-drug delivery system has a good therapeutic effect on tumors, and this study provides significant insights into the role of different subcellular organelles in inhibiting tumor growth and metastasis and inspires researchers to develop highly effective cancer therapeutic strategies through subcellular organelle targeted drugs.

Keywords: breast cancer metastasis, gambogic acid, paclitaxel, mitochondria, nucleus

Introduction

Breast cancer is one of the most common malignant tumors, and its morbidity and mortality rank first among all kinds of tumors in women.[1,2] As an independent clinicopathological type of breast cancer, the incidence of triple-negative breast cancer (TNBC) accounts for about 12–17% of breast cancers.[3] TNBC patients are characterized by a high degree of malignancy, strong drug resistance, short overall survival, high rate of early recurrence, poor prognosis, strong invasion ability and other clinical characteristics, which are difficult to treat and lack specific targets. Chemotherapy is still the main method of tumor treatment including TNBC, which can significantly prolong the survival time of tumor patients. However, chemotherapy drugs have some problems such as short metabolism time, poor targeting, easy drug resistance

Received: 5 April 2023
Accepted: 21 May 2023
Published: 8 June 2023

Graphical Abstract

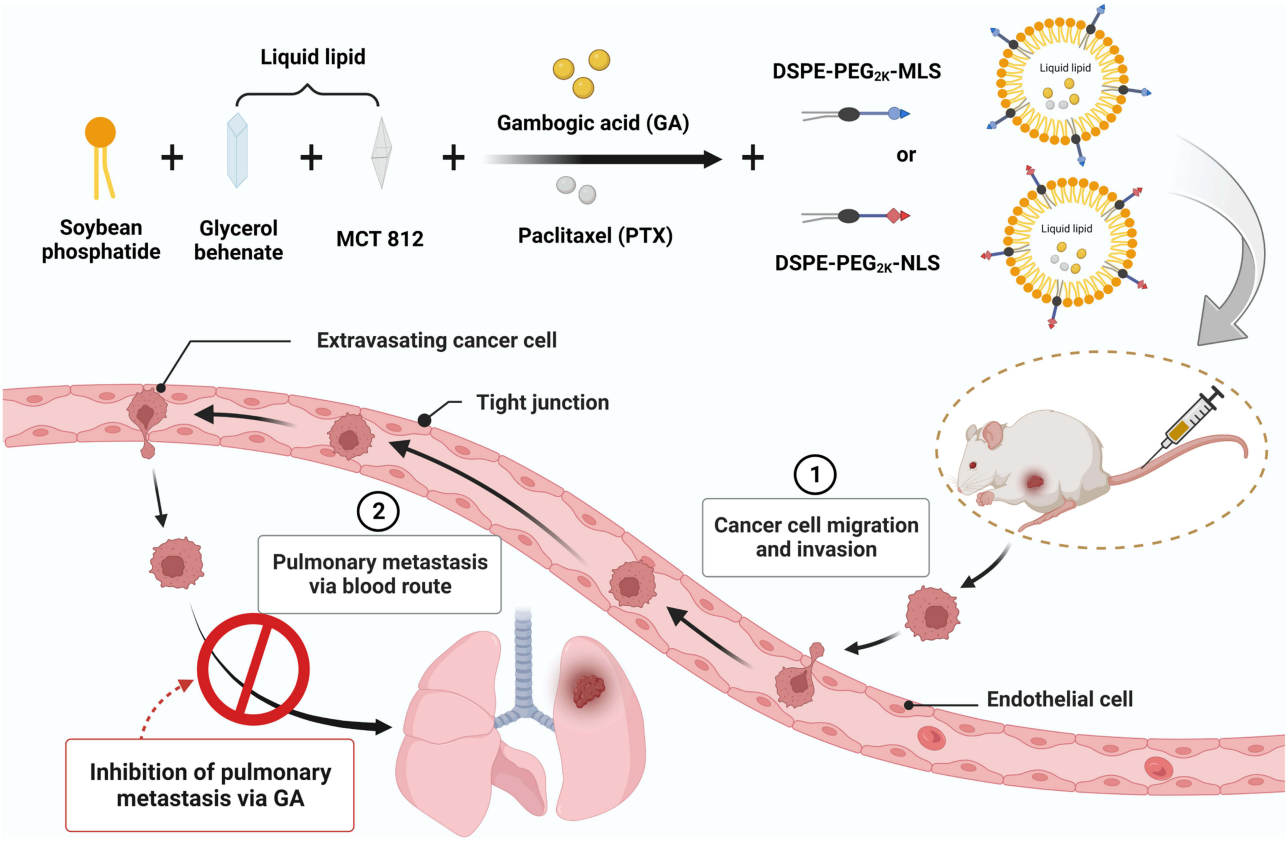

and large side effects.[4] Additionally, according to reports, some chemotherapeutic agents, including Paclitaxel (PTX), which contributed to the infiltration and extravasation of cancer cells.[5,6]

PTX is a classic microtubule inhibitor that facilitates G2/M phase arrest and mitotic cell death.[7–9] Moreover, PTX can activate apoptosis by reducing mitochondrial membrane potential and opening mitochondrial permeability conversion pores, and can alter the tumor metastatic microenvironment (TMEM) and promote distant metastasis of breast cancer, increasing the risk of metastatic dissemination,[10] which not only helps cancer cells escape from the primary site, but also directly affects the lung, altering the microenvironment of the lung and helping breast cancer cells colonize the lung.[11] Hence, reducing its role in promoting pulmonary metastasis is a key problem at present. Moreover, for cancer, a malignant disease caused by many complex factors, the treatment effect of single-target chemotherapy is often unsatisfactory. Therefore, combination therapy has become a new strategy for cancer.[12–15]

Gambogic acid (GA) is a natural compound isolated from gamboge, which can inhibit cancer cell adhesion, migration and invasion in vitro.[16] Low concentrations of GA can inhibit the invasion of breast cancer cells without affecting cell viability, and induce cell apoptosis through ROS (Reactive oxygen species) accumulation and activation of the mitochondrial apoptotic pathway.[17] Therefore, the combination of these two drugs, can achieve their synergistic anti-tumor effect. We have previously encapsulated the two drugs in nanostructured lipid carriers (NLC) at an optimal ratio (GA: PTX = 1.18: 1), and achieved good anti-tumor effects.[18] Therefore, on this basis, the NLC was modified with different subcellular organelle targeted peptides to explore the role of subcellular organelle in apoptosis and pulmonary metastasis of triple-negative breast cancer.

Nowadays, subcellular organelle targeted nano-formulations for cancer treatment are receiving increasing attention owing to their benefits of precise drug delivery, maximized therapeutic index, and reduced off-target side effects. The

nucleus and mitochondria, as the main subcellular organelles, are the significant organelles responsible for maintaining cell operation and metabolism. They can be involved in many essential physiological and pathological processes such as cell proliferation, organism metabolism, and intracellular transportation and play a critical role in regulating cell biology.[19,20] The dysfunction of these organelles can lead to various abnormal regulations and a variety of diseases. For example, any turbulence in the nucleus may generate aberrant regulations of cell activity and even lead to the programmed death of the cell.[21] In addition, mitochondrial dysfunction is associated with a variety of pathological symptoms, such as cardiovascular, neurodegenerative diseases and cancers.[19,22] Therefore, the concept of organelle and subcellular organelle targeted is gaining increasing attention in the near future.

The α-helical amphipathic peptide DKLAKLAKKLAKLAK, as the mitochondrial localization peptides (MLS), was originally designed as a synthetic antibacterial peptide that disrupts the bacterial cell membrane, is non-toxic, positively charged, and has pro-apoptotic abilities.[23] It has been experimentally confirmed that MLS can specifically target mitochondria and destroy their membranes. The peptide activated mitochondria-dependent cell-free apoptosis in a system composed of mitochondria suspended in cytosolic extract, as measured by characteristic caspase-3-processing from an inactive zymogen to active protease.[24] In addition, MLS promotes cellular uptake by nano delivery systems (NDS), Improving the efficiency of suppression of TNBC in vitro and in vivo.[25,26] This is mainly because the six lysine residues in the MLS could be kept intact with the tumor cell membranes and mitochondria membranes by electrostatic attractions and hydrogen bonding to facilitate drugs internalization.[27,28] The nuclear localization sequence (NLS), CGGGPKKKRKVGG, represents a group of oligopeptides that containing short amino acid sequences. It has been reported that NLS can act as a carrier to guide proteins into the nucleus through nuclear pore complexes, and experiments have also shown that NLS-modified NDS can accurately deliver drugs to the nucleus, indicating that they have a good nuclear targeting effect.[29,30]

Based on the above mechanism, we proposed to inhibit tumors and reduce metastatic cancer cells by targeting different organelles. NLC is powerful tools for multidrug combination therapy because they can encapsulate various drugs on a single carrier and control their release spatially and temporally.[31] Therefore, NLC composed of the insoluble anti-tumor component GA and PTX and lipid was synthesized. The NLC was functionalized with MLS and NLS, respectively. Finally, the tumor targeted, anti-tumor and inhibition metastasis effects of NLC were investigated in vitro and in vivo. In this research, we used subcellular organelle targeted peptides to improve the tumor-targeting ability of NLC and is promising for promoting highly efficient nanotherapeutic approaches for cancer treatment.

Materials and Methods

Materials, Cell Lines and Animals

PTX with a purity of over 98% was purchased from Shanghai Yuanye Bio-Technology Co., Ltd (Shanghai, China); GA with a purity of over 98% was obtained from Chengdu Herb-purify Co., Ltd (Chengdu, China); Taxol® (30 mg/5 mL) was bought from Hospira Australia Pty Ltd; DSPE-PEG_{2K}-COOH and soybean phosphatide were obtained from AVT (Shanghai, China); MLS and NLS (Figure S1 MALDI–TOF mass spectra of DSPE-PEG_{2K}-COOH, MLS, DSPE-PEG_{2K}-MLS, NLS, DSPE-PEG_{2K}-NLS) were obtained from China peptide Biotech Co. Ltd. (Shanghai, China); Mito-tracker™ Green FM and Mito-tracker™ Deep Red FM was bought from Thermo Fisher (Invitrogen, US); Hoechst 33342 from Sigma-Aldrich (MO, USA); Cyanine 5 (Cy5) was purchased from Lumiprobe (US); Cell Counting Kit-8 (CCK-8) was purchased from Dojindo Laboratories (Kumamoto, Japan); 4T1 cell line and MDA-MB-231 cell line were ordered from American Type Culture Collection (ATCC). Female BALB/c mice (3–5 weeks old females, 18.0 ±2.0 g) were bought from SBF Biotechnology Co., Ltd (Beijing, China). The laboratory animal production license: SCXK (Jing) 2019-0010. All animals were fed in the area of the Animal Experimental Center of Tianjin University of Traditional Chinese Medicine and allowed free access to food and water during the routine day and night cycle. The experiments were carried out after a week of adaptive feeding. The animals were conducted according to the guidelines evaluated and approved by the Ethical Committee of Tianjin University of Traditional Chinese Medicine (Document number: TCM-LAEC2022053).

Preparation of NLC

The emulsification-evaporation method fabricated GA and PTX loaded NLC, the PTX and GA was fixed as the weight ratio was 1:1.8 (PTX: 2.12 mg, GA: 2.5 mg).[18] Briefly, GA, PTX and Soybean phosphatide were dissolved in ethanol; MCT 812 (Miglyol 812, Beijing Feng Li Jing Qi Trading Co., Ltd. China,) and Compritol® 888 ATO (Glycerol behenate, Saint-Priest Cedex, France) were dissolved in chloroform, and the two solutions were mixed to get the oil phase. Myrj 52 (Polyethylene Glycol (40) Monostearate, Saint-Priest Cedex, France) was dissolved in deionized water as the aqueous phase. The oil phase was rapidly added to the aqueous phase under magnetic stirring at 77–80 °C. The solution was stirred continuously to evaporate the organic solvent, then placed it in a refrigerator at 4 °C. After 30 min, measured size, zeta potential, and encapsulation efficiency. For MLS-PTX+GA-NLC and NLS-PTX+GA-NLC, MLS and NLS were dissolved in the chloroform together with ethanol, respectively. Other steps were the same as above. DiR or Cy5 were mixed in ethanol when prepared DiR-NLC or Cy5-NLC.

Characterization of NLC

Particle Size, Zeta Potential and Morphology

Particle size, polydispersity index (PDI), and zeta potential of the PTX+GA-NLC, MLS-PTX+GA-NLC and NLS-PTX +GA-NLC were measured by Malvern particle sizer and Zeta potential analyzer (Malvern Instruments, UK). Transmission electron microscopy (TEM) was used for investigating the morphology of the NLC (JEM-1200EX (120KV), JEOL, Japan).

Determination of Encapsulation Efficiency

The encapsulation efficiency and drug loading of NLC were calculated indirectly by measuring the free drug. Among them, the total concentrations of GA and PTX were determined by adding methanol to demulsify and release the drug by sonicating for 35 min. The concentration of the free drug was determined by collecting the filtrate from the ultrafiltration centrifuge tube. Then the samples were measured by HPLC (LC-20A, Shimadzu, Japan) on a reversed-phase C18 column (250 mm × 4. 6 mm, 5 μm) at 30 °C. The mobile phase contained (A) water, including 0.1% formic acid, and (B) acetonitrile (A:B = 1:9 (GA); A:B = 4:6 (PTX)). The specificity, precision, linearity, repeatability, and stability of the method were validated. The EE% and DL% were calculated by using the following equation:

$$EE\% = (1 - W_{free}/W_{total}) \times 100\%$$

$$DL\% = \frac{W_{total} - W_{free}}{W_{mass}} \times 100\%$$

Where, W_{total} is the total weight of GA and PTX in the NLC, respectively. W_{free} is the weight of unloaded GA and PTX, respectively. W_{mass} is the total weight of solid and liquid lipids.

Differential Scanning Calorimetry (DSC)

The thermal analysis of PTX, GA, Blank NLC, the physical mixture, PTX+GA-NLC, MLS-PTX+ GA-NLC, and NLS-PTX+GA-NLC was performed to investigate the drug state in NLC. The sample powder was placed in a sealed aluminum dish with a hole cover, and the DSC curve was measured at 30–300 °C under the condition of a heating rate of 10 °C/min under the nitrogen gas flow of 20 mL/min (DSC, PerkinElmer Inc. USA).

Fourier Transform Infrared Spectroscopy (FTIR)

Fourier transform infrared spectrometer to record spectra. PTX, GA, Blank NLC, the physical mixture, PTX+GA-NLC, MLS-PTX+ GA-NLC, and NLS-PTX+GA-NLC and an appropriate amount of KBr were ground, crushed and pressed into a disc in a mortar, then measured in the scan range of 400 cm^{-1} to 4000 cm^{-1}.[32]

XRD Analysis

PXRD patterns of the different samples were acquired from an X-ray diffractometer (D8 advance, Bruker-axs, Germany). Samples of PTX, GA, Blank-NLC, the physical mixture, PTX+GA-NLC, MLS-PTX+GA-NLC, NLS-PTX+GA-NLC

were detected under the following conditions: Cu-Kα tube radiation source, tube pressure 40 kV, current 200 mA, scanning in the 2θ range 5–75°, and scanning rate 5°/min.

Subcellular Organelle Targeting

Confocal laser scanning microscopy (CLSM) was used to track the subcellular localization of NLC (the fluorescent dye, Cy5, to visualize the NLC). CLSM observed that Cy5-Sol, Cy5-NLC, MLS-Cy5-NLC and NLS-Cy5-NLC were located in the mitochondria or nucleus of the MDA-MB-231 cells (the concentration of Cy5 was 100 nmol/L). Cells (8.0×10^4 cells/well) were seeded on a glass slice (d = 18 mm) and incubated for 24 hours. The cells were incubated with a complete culture medium containing different NLC for 2 h and 6 h. Then washed twice with cold PBS, and 1.0 μg/mL Hoechst 33342 and 100 nmol/L Mito-tracker™ green FM per well were added to each well to stain the nuclei and mitochondria, respectively. After 30 min, the stained cells were washed with PBS two times and observed by CLSM at excitation wavelengths of 646 nm, 346 nm, and 490 nm, and emission wavelengths of 662 nm, 460 nm, and 516 nm for Cy5, Hoechst 33342 and Mito-tracker™ green FM, respectively. Image J software was used to calculate the fluorescence value of each dye.

Cellular Uptake

The cellular uptake behavior of the NLC preparations was tested on MDA-MB-231 and 4T1 cells, and they loaded the fluorescent dye, Cy5, to visualize the NLC. MDA-MB-231 and 4T1 cells were seeded in 96-well culture plates at a density of 1.2×10^4 cells/well and 1.0×10^4 cells/well, respectively. After 24 h, the cells were treated with Cy5-Sol, Cy5-NLC, MLS-Cy5-NLC and NLS-Cy5-NLC at their non-toxic concentration for 2 h and 6 h (the concentration of Cy5 was 100 nmol/L). After washing three times with cold PBS, then added 100 μL 1.0 μg/mL Hoechst 33342 per well to stain the nuclei. Cells were cultured at 37 °C for 30 min in the dark. Then they were washed three times with 100 μL PBS, and 100 μL of RMPI-1640 medium or DMEM medium were added to each well. The fluorescent images were captured with an InCell Analyzer 2500 High-connotation Cell Imaging Analysis system (GE Healthcare, USA). The mean fluorescence intensity values of images of each well were calculated using IN Cell Developer Toolbox software.

In vitro Cytotoxic Activity

The CCK-8 assays were performed to evaluate the cytotoxicity of different NLCs, 4T1 and MDA-MB-231 cell lines, these two types of cells with a density of 5.0×10^3/well and 6.0×10^3/well were seeded into 96-well plates, respectively. After 24 hours, they were separately cultured with different concentrations of GA and PTX. 24 hours later, 100 μL 10% CCK-8 solution was added to each well after removing the medium, and then the cells were incubated for 45 min. The absorbance of each well at 450 nm was measured by a microplate reader (TECAN, Switzerland). Cell viability was calculated as:

$$Cell\ viability(\%) = \left(\frac{A_s - A_b}{A_c - A_b}\right) \times 100\%$$

Where, A_s, A_c and A_b refer to the absorbance of the experimental wells, the control wells, and the blank wells, respectively.

Detection of Mitochondrial Membrane Potential and Mitochondrial Distribution

The main mechanism of apoptosis induced by GA is through the change of mitochondrial membrane permeability mediated by excessive ROS. And PTX can activate apoptosis by reducing mitochondrial membrane potential and opening mitochondrial permeability conversion pores. To measure the changes of mitochondrial membrane potential and mitochondrial distribution, MDA-MB-231 cells were seeded in a 96-well plate at a density of 1.2×10^4 cells per well and cultured for 24 h. The medium was then replaced with 100 μL of PBS, PTX+GA-Sol, PTX+GA-NLC, MLS-PTX+GA-NLC or NLS-PTX+GA-NLC at the same equivalent GA concentration of 0.3 μg/mL and cultured for 6 h. After washing with PBS twice, and the cells were stained with JC-1 or Mito-tracker™ Deep Red FM and measured by CLSM (the concentrations of JC-1 and Mito-tracker™ Deep Red FM in all samples were 5 μmol/ and 100 nmol/L, respectively). Calculate the fluorescence intensity using Image J software.

Scratch Wound-Healing, Cell Migration and Invasion

Scratch wound healing is a classic in vitro cell model experiment to detect the migration ability of tumor cells. MDA-MB-231 cells were seeded on a 6-well culture plate. After the cells grew to form a dense membrane monolayer, the middle of the six-well plate filled with MDA-MB-231 cells was scratched with a 200 μL gun head, and the images were observed and photographed under a light microscope by EVOS XL Imaging System (Thermo, US). After the addition of PBS, Blank-NLC, GA-Sol, GA-NLC, MLS-GA-NLC and NLS-GA-NLC (GA with the concentration of 0.1, 0.2, 0.3 μg/mL), the cells were cultured in the cell medium for 48 h. The wound healing of MDA-MB-231 cells in all groups was observed again under the light microscope and photographed. Image J software was used to calculate the scratch area before and after the experiment.

To further research the inhibitory effect of GA on cell migration, trans-well plates (24-well, 8.0 μm pore size, transparent PET membrane, Corning, USA) were used to study cell migration. Specific operations were as follows: MDA-MB-231 cells were suspended in a serum-free medium containing 0.3 μg/mL GA, and then the cell suspension containing GA was added into the upper chamber of the trans-well chamber, with the amount of 0.2 mL per well. At the same time, 0.8 mL of complete medium containing 30% FBS corresponding to the same concentration of GA was added to the lower chamber (n = 3). Incubated at 37 °C with 5% CO_2 for 24 h, the residual liquid in the upper chamber was removed, the upper chamber was cleaned with PBS solution, and gently wiped off the non-migrated cells. Then, the migrating tumor cells were stained with 0.1% crystal violet for 30 min. After the staining, photos were taken and recorded. The migrating cells were counted as follows: the crystalline violet was completely dissolved by ultrasonic treatment with 35% acetic acid for 10 min. Then 200 μL of solvent was placed in a 96-well plate, and the absorbance at 570 nm was measured with a multifunctional microplate reader. And the other groups were compared with the control group.

In the invasion experiment, matrigel preparation was required in advance. Matrigel can be gelatinized quickly at 22–35 °C, so it should be placed in a refrigerator at 4 °C overnight to reach the resolution state. In addition, all EP tubes, pipettes, and gun heads used in the experiment should be placed in a 20 °C refrigerator overnight for pre-cooling. Matrigel was diluted to 1:4 with a pre-cooled serum-free medium for subsequent experiments. The upper compartment was then coated with Matrigel to simulate the invasion of the basement membrane by tumor cells in situ. The other operations are consistent with the migration experiment.

In-vivo Imaging

Tumor-bearing BALB/c mice were established. Briefly, 2.0×10^7 4T1 cells were subcutaneously inoculated in the left armpit of the mice after wiping them with alcohol cotton. Chosen DiR as a fluorescent probe for labeling NLC to assess tumor targeting efficiency and in-vivo bio-distribution of the preparations. When the tumor volume increased to 200 mm^3 (tumor volume $V = ab^2 / 2$; a: tumor length, b: tumor width), the mice were randomly divided into four groups (n = 3): DiR-Sol, DiR-NLC, MLS-DiR-NLC and NLS-DiR-NLC. Then different formulations were injected via the tail vein at a DiR dose of 0.5 mg/kg. At 1 h, 4 h, 12 h, and 24 h post-injection, each mouse was anesthetized and put in an In-Vivo Imaging System (IVIS; CRi Maestro™ 2 Maestro™ EX-RRO, American) to observe the fluorescence intensity of the tumor site at a wavelength of Ex = 748 nm, Em = 780 nm. The animals were sacrificed after 24 h of imaging, and observed the fluorescence intensity of isolated tissues and tumors.

Inhibition of Tumor Growth and Pulmonary Metastasis in vivo

4T1 cells in logarithmic growth were centrifuged and suspended with PBS. The cell suspension was administered to the left mammary gland of BALB/c female mice at a density of 1.0×10^7 cells per mouse. The mice were observed for 7 days after inoculation and started administering when the tumor volume reaches 100 mm^3. The tumor-bearing mice were randomly divided into seven groups (six mice in each group): the saline group (the blank control group), the Taxol group (the positive drug group), PTX-Sol, PTX+GA-Sol, PTX+GA-NLC, MLS-PTX+GA-NLC, NLS-PTX+GA-NLC. Each group was injected with an equivalent dose of 1.7 mg/kg PTX. The different NLCs were administrated intravenously by the tail vein every two days. During administration, measured the tumor volume and weight every three days using

a Vernier caliper and an electronic scale. The tumor volume was calculated according to the formula: tumor volume = long axis × short axis × short axis/2. After treatment, collected blood and measured the levels of aspartate transaminase (AST), creatinine (CRE), and creatine kinase (CK) to evaluate the effect of the drug on major organs function in mice. CD31 antibody and Terminal deoxynucleotidyl transferase-mediated dUTP-biotin nick end labeling (TUNEL) kit staining were used to observe the proliferative activity and necrosis of tumor tissue.

The inhibition rate of tumor volume (IRTV) and Tumor index (TI) were significant indicators of antitumor efficacy in vivo, used the following formula to calculate:

$$\mathrm{IRTV}\ (\%) = (1 - \mathrm{TV_{test}}/\mathrm{TV_{Sal}}) \times 100\%$$

$$\mathrm{TI} = \mathrm{W_{tumor}}/\mathrm{W}$$

Where, $\mathrm{TV_{test}}$ and $\mathrm{TV_{Sal}}$ are the average tumor volume of the saline group and tested groups. $\mathrm{W_{tumor}}$ represents the tumor weight of each group and W referred to the weight of mice.

After the experiment, the mouse tumor and lung tissue were immersed in 4% paraformaldehyde. The number of lung tumor metastasis was counted by visual method and staining of the histologic sections with H&E. Then the tumor tissues were subjected to immunofluorescence analysis with E-cadherin, matrix metalloproteinase-9 (MMP-9) and BCL-2 antibodies. The C-C chemokine ligand 2 (CCL-2) expression in the lungs was detected by Immunofluorescence analysis. Calculate the fluorescence intensity using Image J software.

Statistical Analysis

The results were expressed as the mean ± standard deviation (SD). The Student's *t*-test was performed for statistical analysis of the different groups. The $P < 0.05$ was taken as statistically significant between the data sets, where all significant values were indicated as follows: $^{*}P < 0.05$, $^{**}P < 0.01$, $^{***}P < 0.001$.

Results

Characterization of NLC

Particle Size, Zeta Potential, and Morphology

The results of particle size and zeta potential determination of each group of preparations are shown in Table 1, Figure 1A and B. The particle size of each preparation was between 15.59 and 20.54 nm, the zeta potential was between −9.78 and 1.50 mV, and the PDI was less than 0.300. This series of characterization showed that the prepared NLC had a uniform particle size, which can be applied in subsequent studies. The morphology of each preparation was observed by TEM, and the results were shown in Figure 1C, showing that NLC was spherical or spheroid with uniform size distribution.

Entrapment Efficiency and Drug Loading

The EE% and DL% of each group were determined by HPLC method. As shown in Table 2, the entrapment efficiency of GA and PTX in each group were all greater than 90.40% and 85.56%, indicating that there was no significant difference in the entrapment efficiency of the preparations modified with the subcellular organelle targeted peptide. The drug loading of each group did not change much, which further indicated that the subcellular organelle targeted peptide did not affect the drug loading.

Table 1 Mean Particle Size, PDI and Zeta Potential of PTX+GA-NLC, MLS-PTX+GA-NLC and NLS-PTX+GA-NLC (Mean ± SD, n = 3)

Preparation	Size (nm)	PDI	ZP (mV)
PTX+GA-NLC	15.87±0.28	0.24±0.01	−9.32±0.46
MLS-PTX+GA-NLC	19.96±0.58	0.29±0.01	−3.72±0.24
NLS-PTX+GA-NLC	19.80±0.44	0.27±0.03	1.18±0.15

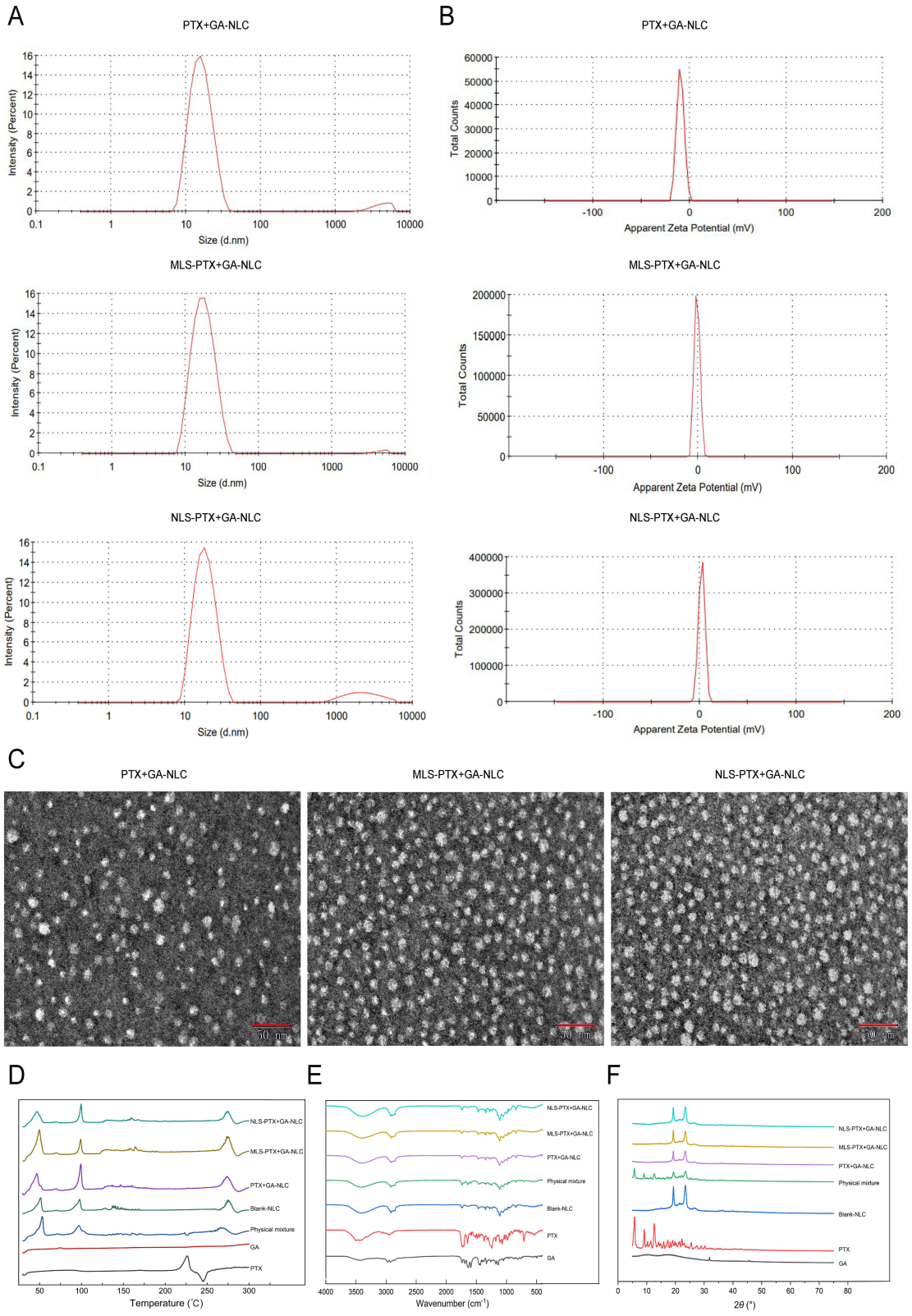

Figure 1 (**A**–**C**) Characteristics of PTX+GA-NLC, MLS-PTX+GA-NLC and NLS-PTX+GA-NLC. (**D**–**F**) DSC, FTIR and XRD of different preparations, respectively.

Differential Scanning Calorimetry (DSC)

DSC can investigate the presence of drugs in the matrix according to different melting points and melting enthalpy.[33] The results of DSC determination were shown in Figure 1D. The melting endothermic peaks of GA and PTX appear at 75 °C

Table 2 EE% and DL% of PTX+GA-NLC, MLS-PTX+GA-NLC and NLS-PTX+GA-NLC (Mean ± SD, n = 3)

Preparations	EE_{GA}%	DL_{GA}%	EE_{PTX}%	DL_{PTX}%
PTX+GA-NLC	95.53±2.30	7.14±0.12	89.27±2.85	5.50±0.19
MLS-PTX+GA-NLC	93.07±2.67	6.43±0.31	87.26±1.70	5.10±0.84
NLS-PTX+GA-NLC	94.69±1.28	6.86±0.03	88.44±0.89	5.43±0.06

and 225 °C, respectively, which are the characteristic peaks of GA and PTX. The characteristic peaks of GA and PTX disappeared in Blank-NLC and drug-loaded NLC, indicating that GA and PTX were encapsulated in the NLC in an amorphous form.

Fourier Transform Infrared Spectroscopy (FTIR)

FTIR results were shown in Figure 1E, GA showed characteristic bands, the C=O bond was extended at 1632.90 cm^{-1}, and the C=C bond was extended at 1593.72 cm^{-1}. The infrared characteristic peak of PTX includes the stretching vibration peak of the -OH at 3411.65 cm^{-1}, the stretching vibration peak of the C=C at 1734.32 cm^{-1}, the stretching vibration of the N-H at 1646.51 cm^{-1}, and the stretching vibration peak of the C-O at 1072.90 cm^{-1}. Characteristics of GA and PTX in the NLC band disappear, as the literature reported that the characteristics of the single drug band will disappear when preparation form.[34] It is suggested that the drug may exist in the lipid matrix.

XRD Analysis

XRD was used to obtain more information on crystal structural properties. Figure 1F showed the comparative XRD patterns: GA, PTX, Blank-NLC, the physical mixture, PTX+GA-NLC, MLS-PTX+GA-NLC, and NLS-PTX+GA-NLC. And there were obvious characteristic peaks of PTX at a diffraction angle (2θ) of 5.759°, 9.128° and 12.614°, the characteristic peaks of GA at a diffraction angle (2θ) of 31.854° and 45.037°. The freeze-dried Blank-NLC had obvious characteristic peaks at a diffraction angle (2θ) of 19.293°, 23.461° and 26.362°. These characteristic peaks were observed in the freeze-dried samples of the physical mixtures, indicating that GA and PTX existed as a crystalline state in the physical mixture. In PTX+GA-NLC, MLS-PTX+GA-NLC and NLS-PTX+GA-NLC samples after freeze-drying, the characteristic peaks of GA and PTX disappeared, which confirmed that GA and PTX were encapsulated in the nanostructured lipid carrier, and there was no crystallisation of drug inside the lipid nanocarrier matrix, indicating the change of GA and PTX from crystalline nature to an amorphous state.[35]

Subcellular Organelle Targeting

As shown in Figure 2, the red fluorescence signal entering the nucleus and mitochondria of the MLS-Cy5-NLC and NLS-Cy5-NLC groups was stronger than that in the unmodified group, while the fluorescence intensity of Cy5-Sol was the weakest. The results showed that NLC was easier to accumulate in cells than free drugs. More importantly, the results also suggested that subcellular organelle targeted peptides facilitated NLC entry into cells and accurately delivered to different subcellular organelles. This laid a foundation for the later use of subcellular organelle targeted peptides to accurately deliver drugs to tumor subcellular organelles to achieve anti-tumor proliferation and induce apoptosis.

Cellular Uptake

As shown in Figures 3A and B and S2 and S3, after incubation of MDA-MB-231 and 4T1 cells for 2 h and 6 h, it was observed that the red fluorescence signals of Cy5-NLC, MLS-Cy5-NLC and NLS-Cy5-NLC were much stronger than that of Cy5-Sol, and the longer the incubation time, the higher the fluorescence intensity. The uptake capacity of NLCs at 2 h and 6 h was significantly stronger than that of Cy5-Sol, and the fluorescence uptake was NLS-Cy5-NLC> MLS-Cy5-NLC> Cy5-NLC> Cy5-Sol, indicating that nano-preparations could increase cellular uptake of Cy5, and after subcellular organelle targeted peptide modification, they could further enhance the uptake of nano-preparations. Statistical analysis showed that the fluorescence intensity of cells at different time points of each group of preparations was statistically significant. The above results may be due to the fact that Cy5-Sol enters cells through passive diffusion mechanisms,

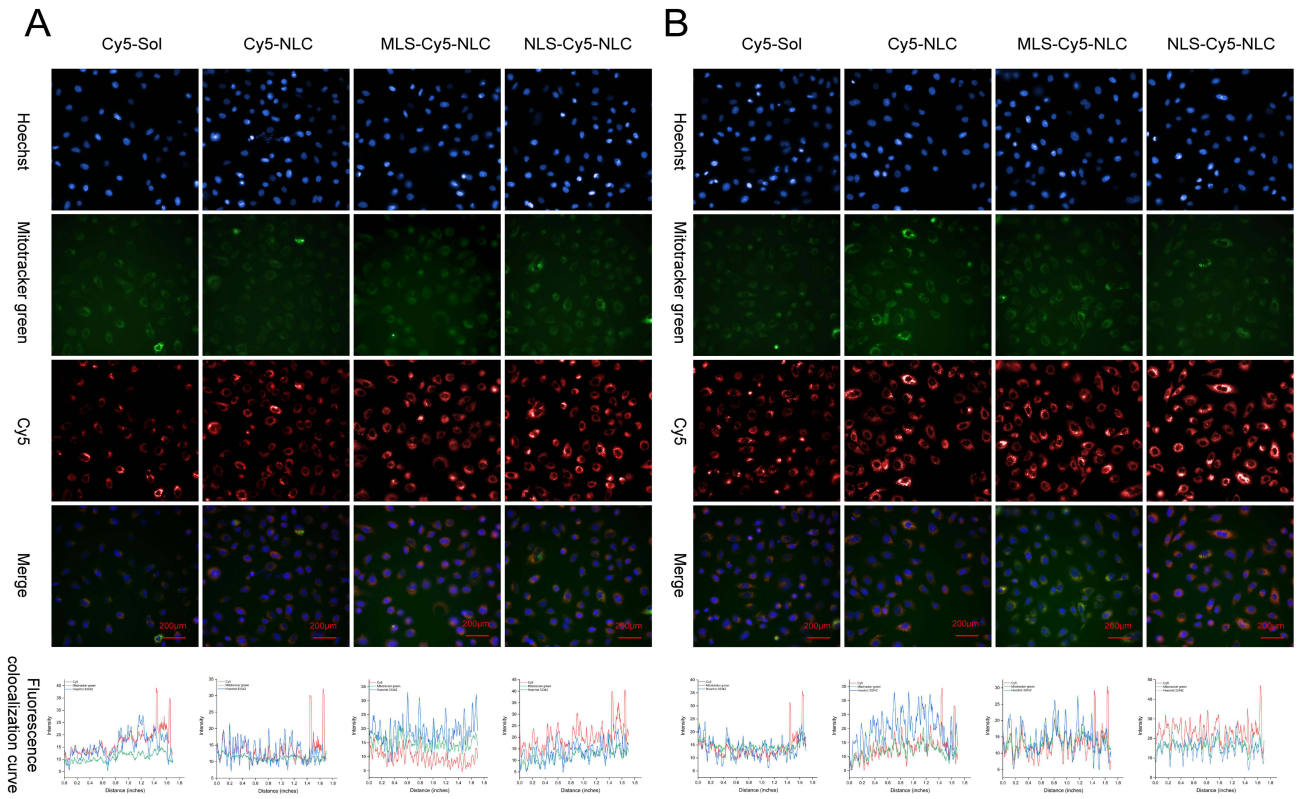

Figure 2 The pictures of Cy5-Sol, Cy5 labeled NLC and subcellular organelle targeted peptide modified Cy5 labeled NLC (Cy5 at the concentration of 100 nmol/L, (**A**) 2 h, (**B**) 6 h. Scale bar = 200 μm).

Cy5-NLC may enter cells through non-specific endocytosis mechanisms, and subcellular organelle targeted peptide modifiers enter cells through peptide-mediated active targeted endocytosis. In addition, the results showed that NLS-Cy5-NLC had the strongest uptake ability of tumor cells, indicating that NLS could help nano-preparations enter the nucleus through nuclear pores.

Cytotoxic Activity Study

Furthermore, as shown in Figure 3C and D and Table 3, 4T1 cells were easy to tolerate GA and PTX more than MDA-MB-231 cells. This may be because human cells are more sensitive to anti-tumor drugs. In 4T1 cells, the half inhibitory concentrations of GA-Sol, PTX+GA-Sol, PTX+GA-NLC, MLS-PTX+GA-NLC and NLS-PTX+GA-NLC were 0.49 ±0.02 μg/mL, 0.41±0.04 μg/mL, 0.34±0.03 μg/mL, 0.26±0.01 μg/mL, and 0.24±0.02 μg/mL, respectively. In MDA-MB-231 cells, the half inhibitory concentrations of GA-Sol, PTX+GA-Sol, PTX+GA-NLC, MLS-PTX+GA-NLC and NLS-PTX+GA-NLC were 0.70±0.01 μg/mL, 0.63±0.02 μg/mL, 0.30±0.01 μg/mL, 0.28±0.01 μg/mL, and 0.25±0.01 μg/mL, respectively. In addition, subcellular organelle targeted peptide modified nanoparticles had a strong inhibitory effect on the growth of cells. More importantly, NLS-PTX+GA-NLC can effectively inhibit the proliferation, proving the universal applicability of NLS in the treatment of breast cancer.

Detection of Mitochondrial Membrane Potential and Mitochondrial Distribution

Mitochondrial membrane potentials of MDA-MB-231 cells after various treatments were assessed by staining with JC-1, which forms J-aggregates with red fluorescence at high mitochondrial membrane potentials, and remains a monomer with green fluorescence at low mitochondrial membrane potentials. Thus, mitochondrial membrane potential can be assessed by observing the relative levels of green and red fluorescence intensities. As depicted in Figure 3E and F, all the cells treated with different formulations exhibited lower mitochondrial membrane potentials than the control ones. Notably, the

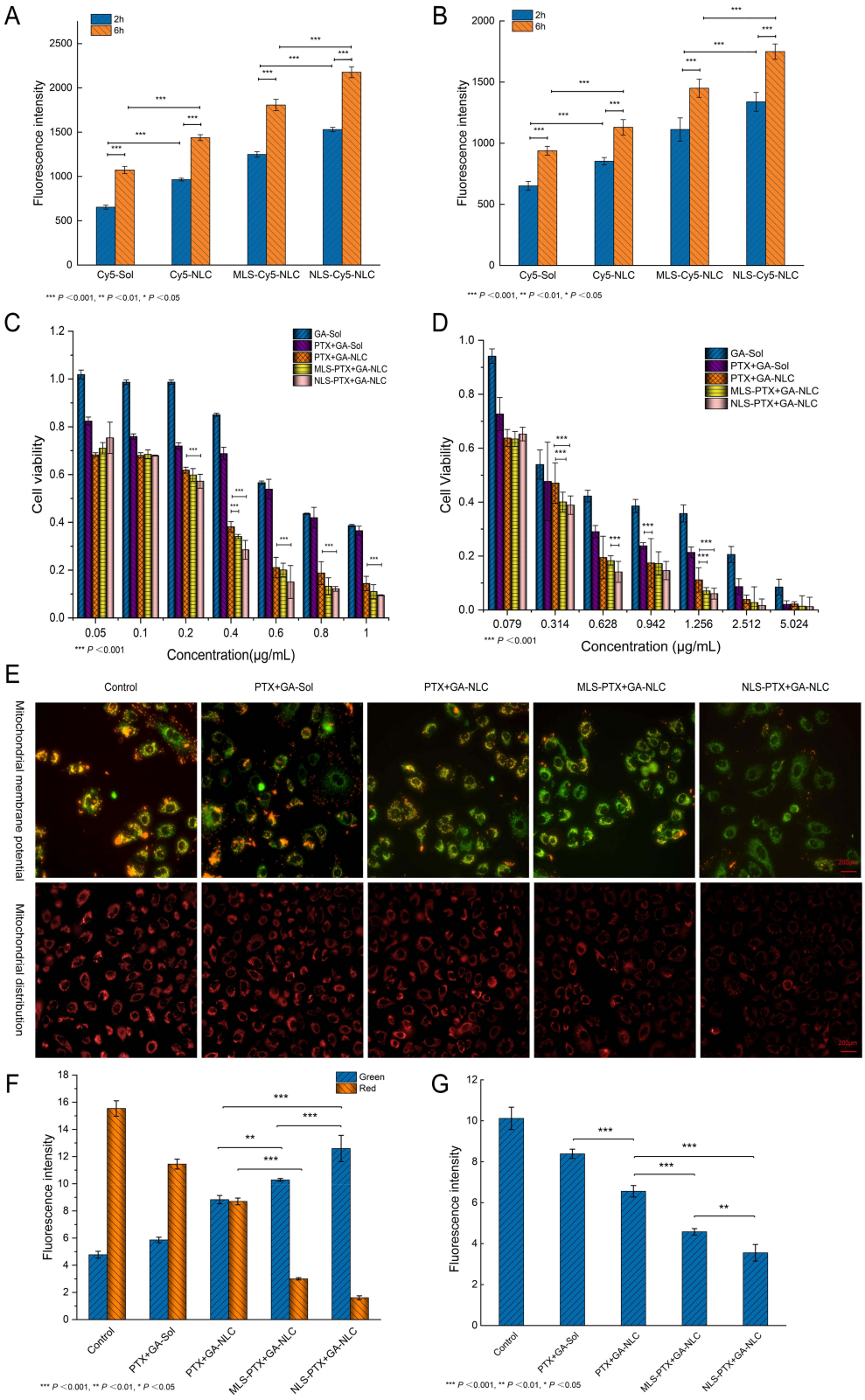

Figure 3 (**A** and **B**) The fluorescence intensity of Cy5-Sol, Cy5 labeled NLC and subcellular organelle targeted peptide modified Cy5 labeled NLC (Cy5 at the concentration of 100 nmol/L, (**A**) MDA-MB-231 cells, (**B**) 4T1 cells). (**C** and **D**) The cell viability of different formulations ((**C**) MDA-MB-231 cells, (**D**) 4T1 cells). (**E**) Mitochondrial membrane potentials and distribution of MDA-MB-231 cells treated with different formulations for 6 h (Scale bar = 200 μm). (**F**–**G**) The fluorescence intensity of mitochondrial membrane potentials and mitochondrial distribution. ***P < 0.001, **P < 0.01, results were expressed as mean ± SD, n = 6.

https://doi.org/10.2147/IJN.S413680 DovePress

Table 3 The Half Maximal Inhibitory Concentration (IC50) of GA-Sol, PTX +GA-Sol, PTX+GA-NLC, MLS-PTX+GA-NLC and NLS-PTX+GA-NLC (Mean ± SD, n = 6)

Preparations	$IC50_{4T1}$ (μg/mL)	$IC50_{MDA\text{-}MB\text{-}231}$ (μg/mL)
GA-Sol	0.49±0.02	0.70±0.01
PTX+GA-Sol	0.41±0.04	0.63±0.02
PTX+GA-NLC	0.34±0.03	0.30±0.01
MLS-PTX+GA-NLC	0.26±0.01	0.28±0.01
NLS-PTX+GA-NLC	0.24±0.02	0.25±0.01

cells treated with NLS-PTX+GA-NLC had the most vigorous green fluorescence intensities, suggesting the lowest mitochondrial membrane potential and the ability to induce apoptosis is the strongest.[36]

Subsequently, the intracellular distribution of mitochondria was investigated through staining with Mito-tracker ™ Deep Red FM, which has red fluorescence. The number of mitochondria is related to the activity of cells. The less the number of mitochondria, the fewer living cells. As shown in Figure 3E and G, all the cells treated with different formulations exhibited a reduced distribution of red fluorescence. The NLS-PTX+GA-NLC group showed the least red fluorescence, indicating the lowest number of mitochondria and the most severe mitochondrial damage, it demonstrated that NLS-PTX+GA-NLC group can better induce apoptosis and had good anti-tumor effect.

Scratch Wound-Healing, Cell Migration and Invasion

In the wound healing experiment, As shown in Figure 4A, the cells in the blank control and Blank-NLC groups grew normally, and the cells almost covered the entire scratch area at 48 h. The results showed that the carrier did not show the effect of anti-tumor migration. Different experimental groups showed different anti-migration effects, indicating that the anti-migration effect was attributed to the anti-metastasis ability of GA. Among them, MLS-GA-NLC and NLS-GA-NLC had stronger anti-migration ability than GA-NLC, while GA-Sol has the weakest anti-migration ability. Under the action of different concentrations of GA, the migration ability was dose-dependent. At the concentration of 0.3 μg/mL, all groups showed the strongest anti-migration ability, and the wound healing rate of NLS-GA-NLC was the lowest (28.14%). Therefore, 0.3 μg/mL GA concentration was selected for the follow-up trans-well experiment.

As shown in Figure 4B, MDA-MB-231 cells in the control group almost covered the whole lower surface of the upper chamber, while the ability of cell migration and invasion in the experimental group decreased to varying degrees. GA-Sol has low anti-migration and anti-invasion ability, whereas GA-NLC significantly delayed cell migration and invasion. MLS-GA-NLC and NLS-GA-NLC showed stronger anti-migration and anti-invasion ability, among which NLS-GA-NLC had the strongest anti-migration and anti-invasion ability, and the migration rate and invasion rate were 53.59% and 33.45%, respectively (Figure 4C).

In-vivo Imaging

As depicted in Figure 5A, at different time points of 1 h, 4 h, 12 h, and 24 h. Compared with other groups, the MLS-DiR-NLC and NLS-DiR-NLC groups performed the strongest fluorescence signal at the tumor site. At 1 h, strong DiR fluorescence was observed at the tumor tissue site in the NLS-DiR-NLC group, indicating NLS directed the DiR into the cell nucleus through the nuclear pore complexes and accumulated DiR at the tumor site. At 4 h, except for the DiR-Sol group, all the other groups had strong DiR fluorescence at the tumor site, and the fluorescence intensity of the subcellular organelle targeted peptide modified groups was stronger than that of the unmodified groups, indicating that the modified nanoparticles had a particular tumor targeting ability. At 12 h, DiR-Sol group performed a little specific accumulation at the tumor site, the fluorescence intensity of DiR-NLC group decreased at the tumor site and DiR was metabolized gradually. And the fluorescence signal of the MLS-DiR-NLC and NLS-DiR-NLC group was stronger than that of the DiR-NLC group, indicating that the modified nanoparticles exhibited an active targeting effect and could increase the accumulation of the drug in the tumor site. At 24 h, the fluorescence intensity of NLS-DiR-NLC was still stronger than

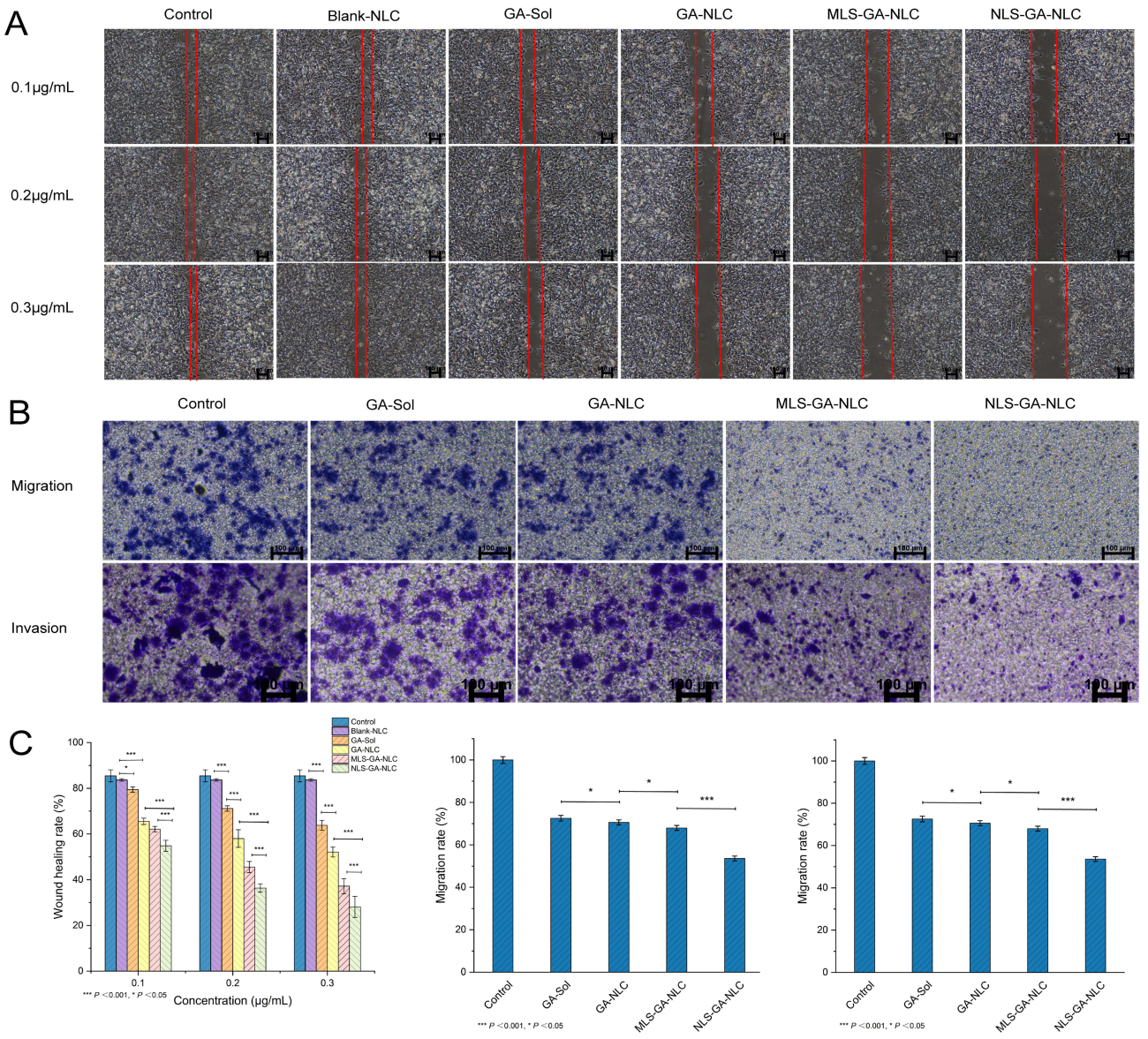

Figure 4 (**A**) The wound healing of different formulations. (**B**) The pictures of migration and invasion. (**C**) Wound healing rate, migration rate and invasion rate. ***P < 0.001, *P < 0.05, results were expressed as mean ± SD, n = 3.

that of other groups. Moreover, as shown in Figure 5B, there were no obvious fluorescence signals in the heart, lungs and kidneys, while the liver and spleen of mice in the NLC groups had certain accumulation of DiR. In additional, According to Figure 5C, the fluorescence intensity of tumor tissue resected from mice after 24 h treatment with different preparations showed that the ex vivo tumor fluorescence signal was the strongest in NLS-DiR-NLC group, further indicating that NLS had good tumor targeting.

Inhibition of Tumor Growth and Pulmonary Metastasis in vivo

According to Figure 6A, the tumor volume of each group increased with the increase of time, while the tumor volume growth rate of the NLCs groups was significantly lower than that of the solution groups, and the tumor volume growth rate of NLCs modified by the subcellular organelle targeted peptide was lower, indicating that the subcellular organelle targeted peptide can more effectively promote the drug to enter tumor cells and make the drug exert a stronger anti-tumor effect. As shown in Figure 6B, the tumor inhibition effect of the PTX+GA-Sol group (25.12%) was slightly better than that of the PTX-Sol group (17.98%), indicating that PTX combined with GA had a synergistic effect. NLC modified by

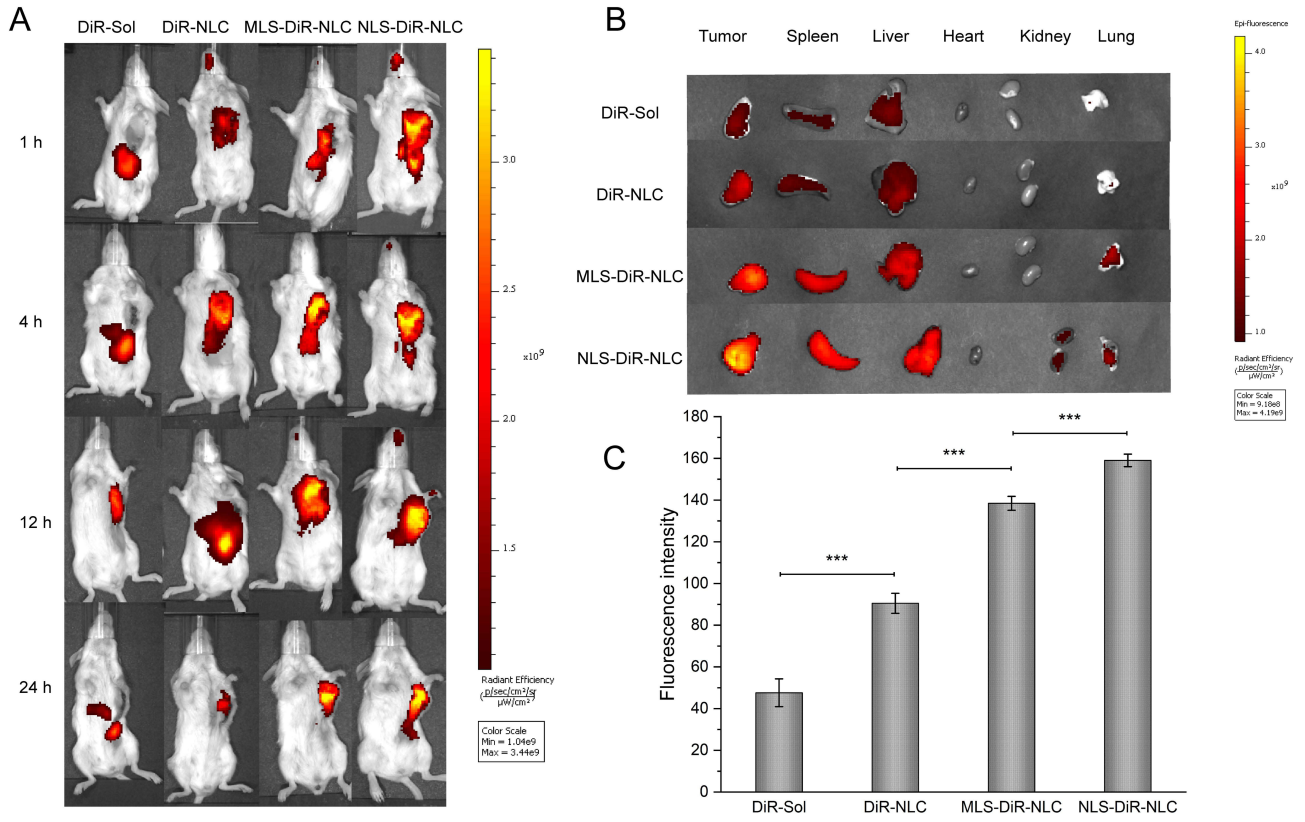

Figure 5 (**A**) Biodistribution of different formulations in 4T1 tumor-bearing mice after intravenous injection for various times, (**B**) The pictures of the tumors and organs removed from mice after 24 h, (**C**) The fluorescence intensity of the tumor tissues excised from the mice after being treated with different formulations at 24 h (***$p < 0.001$, results were expressed as mean ± SD, n = 3).

subcellular organelle targeted peptides showed a stronger tumor inhibition effect, with the TIR of 47.17% and 50.06% for MLS-PTX+GA-NLC and NLS-PTX+GA-NLC, respectively.

The results showed that during the whole experiment, the body weight of mice in the NLS-PTX+GA-NLC group showed a significant downward trend, and the weight of the mice in the other groups did not change significantly (Figure 6C), which may be because NLS mediates the internalization of a larger concentration of drugs into tumor cells, which achieved anti-tumor effect and had certain side effects affecting the diet of mice. The activities of mice in each group were not greatly affected, and the mice in the nano-preparation groups were more active and responsive than those in the solution group, suggesting that nanocarrier encapsulation could reduce the toxicity of drugs.

Moreover, as shown in Figure 6E–G, the effects of drugs on myocytes, especially on cardiomyocytes were evaluated by CK kit, and there was no toxicity among the groups. The results of the AST kit indicated that saline and PTX-Sol showed certain hepatotoxicity, while PTX+GA-Sol did not show hepatotoxicity, indicating that GA can reduce hepatotoxicity. The glomerular filtration capacity was evaluated by the CRE kit to determine the status of renal function, and the results determined that in saline, the CRE levels of PTX-Sol and PTX+GA-Sol were elevated, indicating possible nephrotoxicity. The organ index evaluation of the main organs showed that there was no obvious damage to each organ (Figure 6I). The above results showed that there was no inflammation and toxicity in different NLC groups, indicating that the drug encapsulated by NLC had good biocompatibility and safety.[37]

TUNEL analysis showed that there was little green fluorescence in Saline and PTX-Sol groups, indicating that a small amount of nuclear DNA fragments was produced in the process of apoptosis. The green fluorescence was the strongest in the NLS-PTX+GA-NLC group, which indicated that apoptosis was found in most tumor nuclei. The above results were consistent with the pre-tumor growth (Figure 7A).

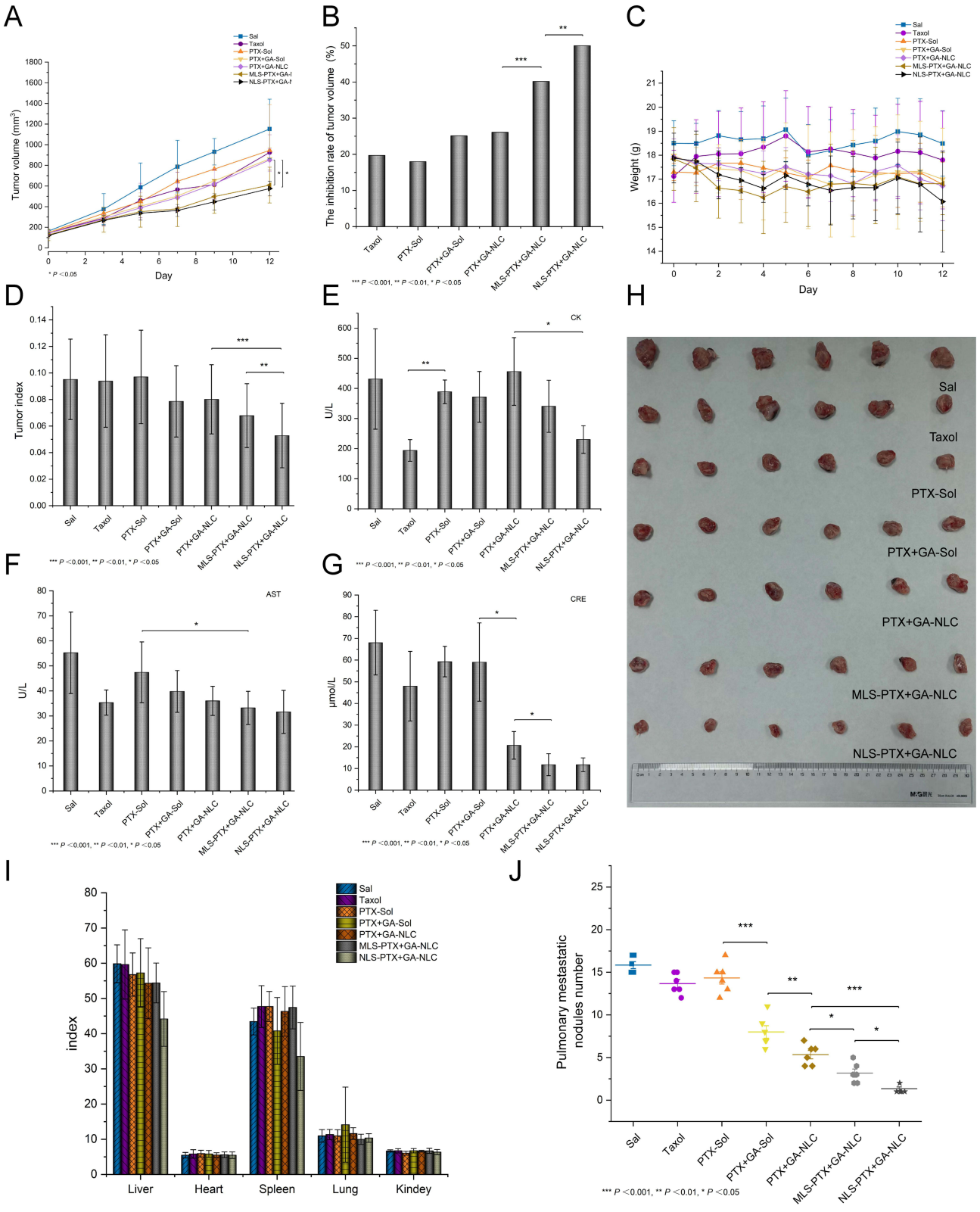

Figure 6 Antitumor effects in vivo. ((**A**) The tumor growth curves. (**B**) The inhibition rate of tumor volume. (**C**) Weight of mice. (**D**) Tumor index. (**E**–**G**) The biochemical markers. (**H**) Photographs of tumors from mice in different treatment groups. (**I**) The index of major organs. (**J**) Number of metastatic nodules in the lung.). ***$p < 0.001$, **$p < 0.01$, *$p < 0.05$, results were expressed as mean ± SD, n = 6.

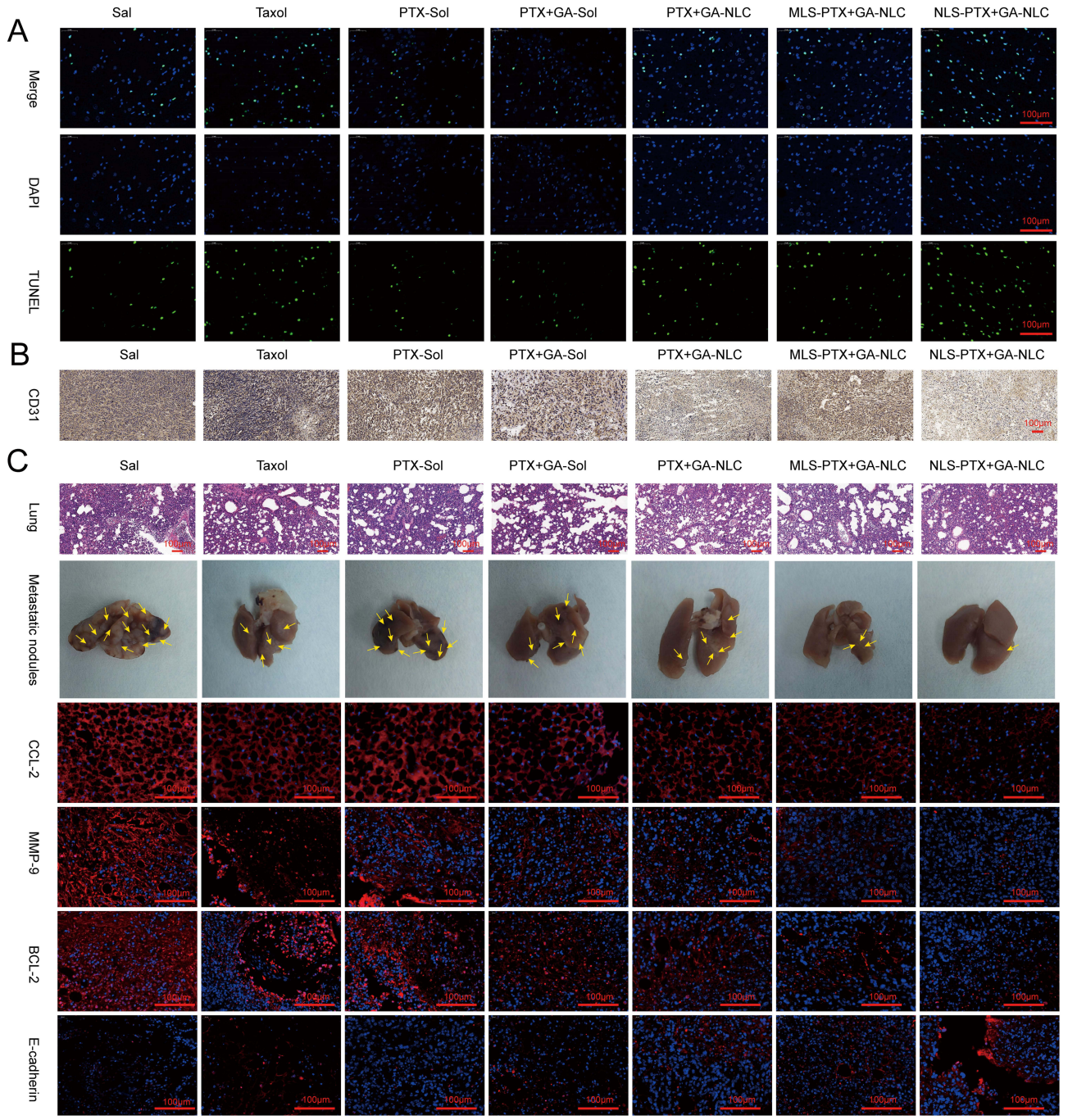

Figure 7 (**A** and **B**) The TUNEL staining and CD31 staining of tumor. (**C**) In vivo antimetastatic effect and mechanism of NLCs (H&E staining of the lung tissues after various treatments, metastatic nodules in the lung, and Immunohistochemical staining of CCL-2 of lung and immunofluorescence staining of MMP-9, BCL-2 and E-cadherin of the primary tumor tissues). Scale bar = 100 μm.

CD31 is an endothelial cell marker used to assess tumor angiogenesis, indicating rapid tumor growth. The results showed that the expression level of CD31 in tumor tissues of the NLS-PTX+GA-NLC group was significantly lower than that of the other groups, indicating that the tumor growth rate was lower than that of the other groups (Figure 7B).

Pulmonary metastasis of 4T1 tumor was determined by image acquisition, pathological examination and immunofluorescence staining of lung tissue. According to Figure 6J, the 4T1 tumor tended to severe pulmonary metastasis. The average number of metastatic nodules in the Saline group was 15.8, and the number of metastatic nodules in the PTX +GA-Sol group (8.0) was less than that in PTX-Sol (14.3) group, indicating that GA could reduce pulmonary metastasis.

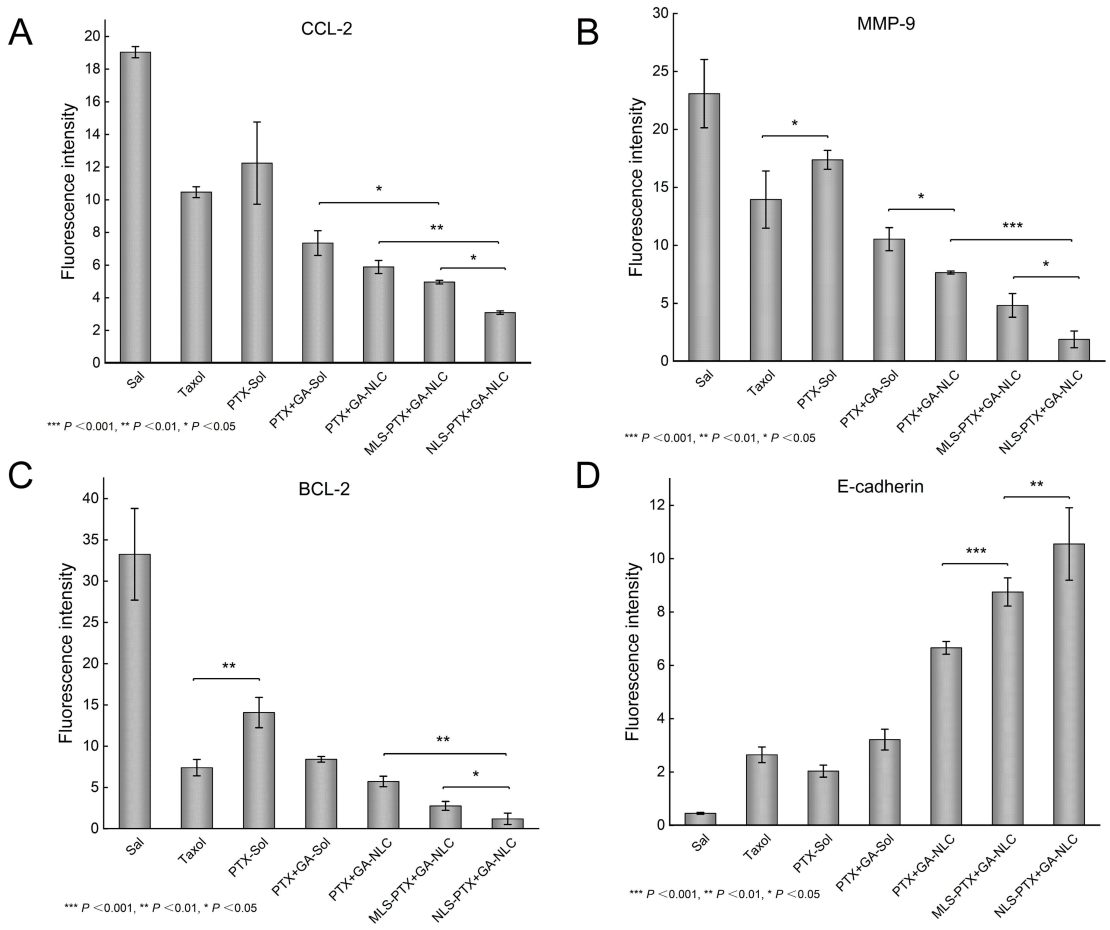

Figure 8 (**A**–**D**) The fluorescence intensity of Immunohistochemical staining of CCL-2 of lung and immunofluorescence staining of MMP-9, BCL-2 and E-cadherin of the tumor tissues.***$p < 0.001$, **$p < 0.01$, *$p < 0.05$, results were expressed as mean ± SD, n = 6.

The average numbers of metastatic nodules of the PTX+GA-NLC, MLS-PTX+GA-NLC, and NLS-PTX+GA-NLC groups were 5.3, 3.2, and 1.3, respectively. The number of pulmonary metastatic nodules in the NLS-PTX+GA-NLC group was the least, indicating that the anti-pulmonary metastasis ability of PTX+GA-NLC was enhanced after NLS targeting.

Therefore, to further explore the mechanism of pulmonary metastasis inhibition, we labeled tumor tissues with MMP-9, BCL-2 and E-cadherin antibodies and performed immunofluorescence staining. According to Figures 7C and 8A–D, it was found that NLCs containing GA down-regulated the expression of MMP-9 and BCL-2 and up-regulated the level of E-cadherin compared with other groups. In addition, the PTX only-containing formulations exhibited higher CCL-2 monocyte levels compared with the saline group, and this elevation could be counteracted by combining GA with PTX, especially when the two drugs were encapsulated in the same carrier.

Discussion

As a malignant tumor, breast cancer is mostly female, and in recent years, it has shown a younger trend. PTX is a commonly used chemotherapeutic drug for the treatment of breast cancer, but it changes the tumor metastasis microenvironment so that cancer cells escape from the primary site and tend to colonize in the lungs.[38] GA can promote the apoptosis of cancer cells by activating the mitochondrial apoptosis pathway, and inhibit the migration and invasion of breast cancer cells without affecting normal cell viability. Based on the above pharmacological effects of GA and PTX, this study co-loaded PTX and GA into nanocarriers (the weights of GA and PTX were 2.5 mg and 2.12 mg, respectively). As a co-loading platform for local or systemic anticancer therapy, nanocarriers can effectively improve the side effects

and poor stability of single chemotherapeutic drugs, and improve the therapeutic effect of multi-drug combination.[39] However, nano-preparations are not easy to target and accumulate in tumor cells. Therefore, we used subcellular organelle targeted peptide modification to improve its ability to target breast cancer cells and increase the uptake of drugs by tumor cells.[40]

About subcellular organelle targeted peptide, Both MLS and NLS are short peptides composed of more than a dozen amino acids, the amino acid sequence of MLS is DKLAKLAKLAKLAK, and the amino acid sequence of NLS is CGGGPKKKRKVGG. The MALDI-TOF reports for two subcellular organelle targeted peptides were shown in Figure S1. In the nanoparticle preparation process, DSPE was divided into hydrophilic end and hydrophobic end because it is structurally similar to SPC. The hydrophilic end of DSPE was linked to PEG_{2K}, which in turn was linked to subcellular organelle targeted peptides. While the core of the nanoparticle was hydrophobic, the hydrophilic ends of SPC and DSPE were distributed on the surface of the nanoparticle, and the above series of distributions ensured that the subcellular organelle targeted peptide was modified on the outer surface of the NLC.

Based to the literature and previous research, we used an improved emulsification-solidification method to functionalize the NLC to prepare PTX+GA-loaded NLC with high drug loading efficiency.[41] The laser particle size analyzer was used for the determination of particle size, the instrument uses the photodetector to collect scattered light intensity data at different angles and distances, and brings in the appropriate scattering theory for data processing, which can obtain the particle size information of the sample. The mean particle size of NLC formulations in this study was about 15.59 to 20.54 nm, within the acceptable range. Besides, the size will not change significantly after modifying with MLS or NLS on the surface of PTX+GA-NLC. It's reported that nanoparticles with a lower absolute value of zeta potential could reduce the clearance by RES, prolonging the blood circulation and enhancing tumor tissue accumulation.[42,43] The PTX +GA-NLC formulations were in an acceptable range with a slight surface charge (−9.78 to 1.33 mV). The size and zeta potential of the nanocarriers play an essential role in biological processes such as biodistribution, blood circulation and uptake by tumor cell.[44,45] Compared with the larger nanocarriers (around 100 nm), a smaller one (approximately 10 nm) performed higher in vitro cytotoxicity and stronger in vivo antitumor efficacy.[46] This lays the foundation for subsequent in vivo and in vitro anti-tumor study.

The selection of fluorescent dyes is an important issue when performing in vitro cell uptake and subcellular organelle targeting assays. Regarding the selection of fluorescent dyes, choose the appropriate fluorescent dye according to your own experimental needs, and the fluorescent dyes commonly used at present are Coumarin 6 (Cou-6),[47] Cy5,[48] fluorescein isothiocyanate (FITC),[49] etc. Since the dyes labeled in this experiment for nucleus and mitochondria were blue and green, there are color restrictions on the choice of dyes. Cou-6 and FITC fluorescence color development are green, there will be color overlap, so Cy5 was finally chosen. Cy5 is an anthocyanin fluorescent dye with an excitation wavelength of 646 nm and an emission wavelength of 662 nm, which has the advantages of good cell tissue permeability, high sensitivity and stable performance, and is widely used in cellular uptake research. The more fluorescent molecules cells absorb, the stronger the fluorescence intensity they exhibit, and choosing the right Cy5 concentration is critical to successful experiments. If the concentration of Cy5 is too small, the cells take less Cy5, the final fluorescence quantitative result value is too small, may cause errors, if the concentration of Cy5 is too large, the fluorescence quantitative value is large and affect the morphology and activity of the cell, and finally the concentration of Cy5 was selected as 100 nmol/L, the concentration will not affect the cell morphology and activity, and the fluorescence intensity meets the needs of the experiment.[48]

In the study of subcellular organelle targeting, the co-localization of subcellular organelles was determined by CLSM. The red, blue and green fluorescent signals represented NLC, nucleus and mitochondria, respectively. Among them, the red fluorescent signal in different positions of the cell represented the entry of NLC into different subcellular organelles of the cell. The overlap of green fluorescence and red fluorescence suggested that the chemical achieved mitochondria targeted localization. The overlap of blue fluorescence and red fluorescence suggested that the chemical achieved nucleus targeted localization. The red fluorescence signal entering the nucleus and mitochondria of the MLS-Cy5-NLC and NLS-Cy5-NLC groups was stronger than that in the unmodified group, while the fluorescence intensity of Cy5-Sol was the weakest. However, the red fluorescence of Cy5 in the NLS modification group overlapped less with the blue fluorescence of Hoechst 33342, which may be at the cellular level, the ability of NLS to mediate Cy5 into the nucleus was not

significant, or it may be that the blue fluorescence of Hoechst 33342 was too strong, blocking the red fluorescence of Cy5, so it needs to be further verified by in vivo targeting experiments in the later stage.

In vivo distribution and tumor targeting were critical parameters for nano-delivery systems. We supposed that the NLC with a smaller size could enhance at the tumor site to effectively kill tumor cells. We compared the tumor-targeting abilities of the subcellular organelle targeted peptide modified groups and unmodified groups in vivo. The fluorescence intensity of NLS-DiR-NLC was always stronger than that of other groups, indicating that NLS had long-term targeting ability in vivo and could mediate the internalization of nanocarriers into the nucleus for a long time. This finding was consistent with the results of in vitro cell uptake experiments and further explained that NLS has good tumor targeting in vivo.

In the process of in vivo efficacy experiments, the mice weight is the most intuitive and easy-to-record evaluation index, and the change of weight also reflects the anti-tumor effect and systemic toxic side effects in a more comprehensive way. And tumor index (TI) is the anti-tumor evaluation index proposed by researchers, with tumor weight exceeding 10% of animal body weight and average tumor diameter of more than 20 mm as the humanitarian endpoint of tumor models in vivo. As shown in Figure 6D, the results showed that the tumor index of mice in each group did not exceed 10%, among which the tumor index of mice in Sal, Taxol and PTX-Sol groups was close to 10%, while the tumor index of mice decreased significantly after GA and PTX were combined, indicating that GA significantly reduced the toxicity of PTX. The tumor index of mice in the subcellular organelle targeted peptide-modified nano-preparation groups was lower, indicating that subcellular organelle targeted peptides could assist drugs to enter the cell. As shown in Figure 6H, it can be seen that the tumor size of the subcellular organelle targeted peptide-modified groups was significantly reduced, indicating that the subcellular organelle targeted peptide can improve the effect of drugs inhibiting tumor growth. Moreover, NLS-PTX+GA-NLC showed the most significant anti-tumor effect during the whole experiment, which may because NLS directed the GA and PTX into the cell nucleus through the nuclear pore complexes, thus mediated drug internalization into tumor cells and increased drug concentration in the tumor. Moreover, unlike the NLC group, the NLS-PTX+GA-NLC and MLS-PTX+GA-NLC groups achieved active targeting through the targeting modified polypeptide, thereby affecting the in vivo biological process of the nanocarriers.

Tumor metastasis is the main factor threatening the survival of cancer patients. During the breathing process, substances in the air enter the lungs to cause an immune response, which is inhibited by the body's protective mechanism, which provides convenient conditions for cancer cell metastasis, so that the immune system does not play a role in cancer cells, and eventually leads to metastases in the lungs. Extracellular matrix and substrate constitute the barrier of tumor metastasis, and its degradation is an important part of tumor invasion and metastasis. Studies have shown that matrix metalloproteinases, as an important enzyme known to degrade extracellular matrix, plays an important role in mediating tumor angiogenesis, metastasis and invasion.[50] The loss or decrease of E-cadherin expression is closely related to tumor metastasis.[51] BCL-2 can prevent the release of cytochrome C from mitochondria to the cytoplasm, thus inhibiting apoptosis.[52]

In vitro anti-metastasis experiments have shown GA had a certain ability to resist migration and invasion, MLS and NLS can target GA to reach different subcellular organelles, MLS-GA-NLC had a good ability to resist migration and invasion because the six lysine residues in the MLS could be kept intact with the tumor cell membranes and mitochondria membranes by electrostatic attractions and hydrogen bonding to facilitate drugs internalization. Most important of all, the reason why NLS-GA-NLC showed the best anti-migration and anti-invasion ability is that NLS acts as a carrier to direct the GA into the cell nucleus through the nuclear pore complexes, thus inducing GA to play a role in anti-migration and anti-invasion.

In vivo anti-lung metastasis experiments, it was found that NLCs containing GA down-regulated the expression of MMP-9 and BCL-2 and up-regulated the level of E-cadherin compared with other groups. The expressions of MMP-9 and BCL-2 in the subcellular organelle targeted peptides modified groups were significantly lower than that in other groups, and the level of E-cadherin was significantly higher than that in other groups, indicating that subcellular organelle targeted peptides had good targeting and could increase the drug concentration of tumor tissues. In addition, chemotherapy based on PTX has been reported to trigger extracellular vesicles that promoted breast tumor metastasis by inducing CCL-2 expression in the lungs.[6] The PTX only-containing formulations exhibited higher CCL-2 monocyte levels compared with the saline group, and this elevation could be counteracted by combining GA with PTX, especially when the two drugs were encapsulated in the same carrier. The expression of the above proteins indicated that GA had

a good effect of inhibiting metastasis, which could effectively antagonize the metastatic effect of PTX, indicating that the combination of the two drugs had synergistic effects.

Conclusion

In this work, GA and PTX were loaded in NLC and then modified with MLS or NLS to prepare MLS-PTX+GA-NLC or NLS-PTX+GA-NLC. The NLCs showed a narrow particle size distribution. As a result, MLS-PTX+GA-NLC or NLS-PTX+GA-NLC effectively enhance subcellular organelle targeted, drug accumulation, and antitumor efficiency of GA and PTX in the breast cancer cells. Meanwhile, NLCs inhibited cells migration via internalizing the GA. The organelle targeted NLCs could significantly inhibit late-stage breast cancer proliferation and reduce metastasis to the lung in vivo. After a series of characterizations, in vivo and in vitro tests, it can be concluded that subcellular organelle targeted could be a potential and suitable strategy for breast cancer.

Abbreviations

AST, Aspartate aminotransferase; CCL-2, C-C chemokine ligand 2; CCK-8, Cell Counting Kit-8; CK, Creatine kinase; CRE, Creatinine; Cy5, Cyanine 5; DiR, 1,10-dioctadecyl-3,3,3,3-tetramethyl indotricarbocyanine Iodide; DL, Drug loading capacity; DMSO, Dimethyl sulfoxide; DSC, Differential scanning calorimetry; DSPE-PEG_{2K}, 1.2-distearoyl-sn-glycero-3-phospho ethanolamine-N-[methoxy(polyethyleneglycol)-2000]; EE, Encapsulation efficiency; GA, Gambogic acid; H&E, Histological Examination; IRBW, The inhibition rate of body weight; IRTV, The inhibition rate of tumor volume; IVIS, In-vivo imaging system; MLS, Mitochondrial localization sequence (DKLAKLAKKLAKLAK); MMP-9, Matrix metalloproteinase-9; Myrj 52, Polyoxyethylene (40) stearate; NLC, Nanostructured lipid carriers; NLS, Nuclear localization sequence (CGGGPKKKRKVGG); PTX, Paclitaxel; PDI, Polydispersity Index; ROS, Reactive oxygen species; TEM, Transmission Electron Microscope; TI, Tumor index; XRD, X-ray diffraction.

Data Sharing Statement

The datasets used and/or analyzed during the current study are available from the corresponding author on reasonable request.

Ethics Approval and Informed Consent

All animal experiments were operated under the approval of the Ethics Committee of Tianjin University of Traditional Chinese Medicine (Ethics authorization number: TCM-LAEC2022053).

Consent for Publication

The Graphical Abstract has been obtained confirmation of publishing rights and license rights of Bio-render, agreement number: EV25CMYMEO.

Funding

This work was supported by Haihe Laboratory of Modern Chinese Medicine science and technology project (22HHZYSS00005) and the National Administration of Traditional Chinese Medicine Young Qihuang Scholar Project.

Disclosure

The authors declare that they have no competing interests in this work.

References

1. Sung H, Ferlay J, Siegel RL, et al. Global cancer statistics 2020: GLOBOCAN estimates of incidence and mortality worldwide for 36 cancers in 185 countries. *CA Cancer J Clin*. 2021;71(3):209–249. doi:10.3322/caac.21660
2. Siegel RL, Miller KD, Fuchs HE, Jemal A. Cancer statistics, 2021. *CA Cancer J Clin*. 2021;71(1):7–33. doi:10.3322/caac.21654
3. Garrido-Castro AC, Lin NU, Polyak K. Insights into molecular classifications of triple-negative breast cancer: improving patient selection for treatment. *Cancer Discov*. 2019;9(2):176–198. doi:10.1158/2159-8290.CD-18-1177

4. Malhotra MK, Emens LA. The evolving management of metastatic triple negative breast cancer. *Semin Oncol*. 2020;47(4):229–237. doi:10.1053/j.seminoncol.2020.05.005
5. Bianchini G, Balko JM, Mayer IA, Sanders ME, Gianni L. Triple-negative breast cancer: challenges and opportunities of a heterogeneous disease. *Nat Rev Clin Oncol*. 2016;13(11):674–690. doi:10.1038/nrclinonc.2016.66
6. Keklikoglou I, Cianciaruso C, Güç E, et al. Chemotherapy elicits pro-metastatic extracellular vesicles in breast cancer models. *Nat Cell Biol*. 2019;21(2):190–202. doi:10.1038/s41556-018-0256-3
7. Hassan MS, Awasthi N, Li J, et al. Superior therapeutic efficacy of nanoparticle albumin bound paclitaxel over cremophor-bound paclitaxel in experimental esophageal adenocarcinoma. *Transl Oncol*. 2018;11(2):426–435. doi:10.1016/j.tranon.2018.01.022
8. Gornstein E, Schwarz TL. The paradox of paclitaxel neurotoxicity: mechanisms and unanswered questions. *Neuropharmacology*. 2014;76 Pt A:175–183. doi:10.1016/j.neuropharm.2013.08.016
9. Bakrania AK, Variya BC, Patel SS. Novel targets for paclitaxel nano formulations: hopes and hypes in triple negative breast cancer. *Pharmacol Res*. 2016;111:577–591. doi:10.1016/j.phrs.2016.07.023
10. Karagiannis GS, Pastoriza JM, Wang Y, et al. Neoadjuvant chemotherapy induces breast cancer metastasis through a TMEM-mediated mechanism. *Sci Transl Med*. 2017;9(397):eaan0026. doi:10.1126/scitranslmed.aan0026
11. Chang YS, Jalgaonkar SP, Middleton JD, Hai T. Stress-inducible gene Atf3 in the noncancer host cells contributes to chemotherapy-exacerbated breast cancer metastasis. *Proc Natl Acad Sci U S A*. 2017;114(34):E7159–E7168. doi:10.1073/pnas.1700455114
12. Plana D, Palmer AC, Sorger PK. Independent drug action in combination therapy: implications for precision oncology. *Cancer Discov*. 2022;12(3):606–624. doi:10.1158/2159-8290.CD-21-0212
13. Yun SH, Kwok SJJ. Light in diagnosis, therapy and surgery. *Nat Biomed Eng*. 2017;1:0008. doi:10.1038/s41551-016-0008
14. Ren X, Wang N, Zhou Y, et al. An injectable hydrogel using an immunomodulating gelator for amplified tumor immunotherapy by blocking the arginase pathway. *Acta Biomater*. 2021;124:179–190. doi:10.1016/j.actbio.2021.01.041
15. Lin Y, Chen X, Yu C, et al. Radiotherapy-mediated redox homeostasis-controllable nanomedicine for enhanced ferroptosis sensitivity in tumor therapy. *Acta Biomater*. 2023;159:300–311. doi:10.1016/j.actbio.2023.01.022
16. Eluard B, Thieblemont C, Baud V. NF-κB in the new era of cancer therapy. *Trends Cancer*. 2020;6(8):677–687. doi:10.1016/j.trecan.2020.04.003
17. Zhen YZ, Lin YJ, Li KJ, et al. Gambogic acid lysinate induces apoptosis in breast cancer mcf-7 cells by increasing reactive oxygen species. *Evid Based Complement Alternat Med*. 2015;2015:842091. doi:10.1155/2015/842091
18. Ma Z, Li N, Zhang B, et al. Dual drug-loaded nano-platform for targeted cancer therapy: toward clinical therapeutic efficacy of multifunctionality. *J Nanobiotechnol*. 2020;18(1):123. doi:10.1186/s12951-020-00681-8
19. Li Y, Heo J, Lim CK, et al. Organelle specific imaging in live cells and immuno-labeling using resonance Raman probe. *Biomaterials*. 2015;53:25–31. doi:10.1016/j.biomaterials.2015.02.056
20. Ma X, Gong N, Zhong L, Sun J, Liang XJ. Future of nanotherapeutics: targeting the cellular sub-organelles. *Biomaterials*. 2016;97:10–21. doi:10.1016/j.biomaterials.2016.04.026
21. Austin LA, Kang B, El-Sayed MA. A new nanotechnology technique for determining drug efficacy using targeted plasmonically enhanced single cell imaging spectroscopy. *J Am Chem Soc*. 2013;135(12):4688–4691. doi:10.1021/ja4011145
22. Mani J, Rout S, Desy S, Schneider A. Mitochondrial protein import - functional analysis of the highly diverged Tom22 orthologue of Trypanosoma brucei. *Sci Rep*. 2017;7:40738. doi:10.1038/srep40738
23. Agemy L, Friedmann-Morvinski D, Kotamraju VR, et al. Targeted nanoparticle enhanced proapoptotic peptide as potential therapy for glioblastoma. *Proc Natl Acad Sci U S A*. 2011;108(42):17450–17455. doi:10.1073/pnas.1114518108
24. Ellerby HM, Arap W, Ellerby LM, et al. Anti-cancer activity of targeted pro-apoptotic peptides. *Nat Med*. 1999;5(9):1032–1038. doi:10.1038/12469
25. Chen T, Chen H, Jiang Y, Yan Q, Zheng S, Wu M. Co-delivery of 5-fluorouracil and paclitaxel in mitochondria-targeted KLA-modified liposomes to improve triple-negative breast cancer treatment. *Pharmaceuticals*. 2022;15(7):881. doi:10.3390/ph15070881
26. Jiang L, Li L, He X, et al. Overcoming drug-resistant lung cancer by paclitaxel loaded dual-functional liposomes with mitochondria targeting and pH-response. *Biomaterials*. 2015;52:126–139. doi:10.1016/j.biomaterials.2015.02.004
27. Li L, Song H, Luo K, et al. Gene transfer efficacies of serum-resistant amino acids-based cationic lipids: dependence on headgroup, lipoplex stability and cellular uptake. *Int J Pharm*. 2011;408(1–2):183–190. doi:10.1016/j.ijpharm.2011.01.051
28. Lai Y, Lei Y, Xu X, Li Y, He B, Gu Z. Polymeric micelles with π-π conjugated cinnamic acid as lipophilic moieties for doxorubicin delivery. *J Mater Chem B*. 2013;1(34):4289–4296. doi:10.1039/c3tb20392a
29. Wang C, Wang B, Zou S, et al. Cyclo-γ-polyglutamic acid-coated dual-responsive nanomicelles loaded with doxorubicin for synergistic chemo-photodynamic therapy. *Biomater Sci*. 2021;9(17):5977–5987. doi:10.1039/D1BM00713K
30. Huo D, Zhu J, Chen G, et al. Eradication of unresectable liver metastasis through induction of tumour specific energy depletion. *Nat Commun*. 2019;10(1):3051. doi:10.1038/s41467-019-11082-3
31. Kemp JA, Shim MS, Heo CY, Kwon YJ. "Combo" nanomedicine: co-delivery of multi-modal therapeutics for efficient, targeted, and safe cancer therapy. *Adv Drug Deliv Rev*. 2016;98:3–18. doi:10.1016/j.addr.2015.10.019
32. Ahmed TA, Alzahrani MM, Sirwi A, Alhakamy NA. Study the antifungal and ocular permeation of ketoconazole from ophthalmic formulations containing trans-ethosomes nanoparticles. *Pharmaceutics*. 2021;13(2):151. doi:10.3390/pharmaceutics13020151
33. Karthik S, Saha B, Ghosh SK, Pradeep Singh ND. Photoresponsive quinoline tethered fluorescent carbon dots for regulated anticancer drug delivery. *Chem Commun*. 2013;49(89):10471. doi:10.1039/c3cc46078a
34. Monschke M, Kayser K, Wagner KG. Influence of particle size and drug load on amorphous solid dispersions containing pH-dependent soluble polymers and the weak base ketoconazole. *AAPS PharmSciTech*. 2021;22(1):44. doi:10.1208/s12249-020-01914-7
35. Padhye SG, Nagarsenker MS. Simvastatin solid lipid nanoparticles for oral delivery: formulation development and in vivo evaluation. *Indian J Pharm Sci*. 2013;75(5):591–598.
36. Jiang W, Yin L, Chen H, et al. NaCl nanoparticles as a cancer therapeutic. *Adv Mater*. 2019;31(46):1904058. doi:10.1002/adma.201904058
37. Lu J, Lou Y, Zhang Y, et al. Paclitaxel has a reduced toxicity profile in healthy rats after polymeric micellar nanoparticle delivery. *IJN*. 2023;18:263–276. doi:10.2147/IJN.S372961
38. Li L, Wu QP, Jiang ZZ. Tumor metastasis induced by chemotherapeutic drugs and mechanism. *Cent South Pharm*. 2022;20(8):1861–1866.

39. Wang N, Cheng X, Li N, Wang H, Chen H. Nanocarriers and their loading strategies. *Adv Healthcare Mater*. 2019;8(6):1801002. doi:10.1002/adhm.201801002
40. Tang SY, Wei H, Yu CY. Peptide-functionalized delivery vehicles for enhanced cancer therapy. *Int J Pharm*. 2021;593:120141. doi:10.1016/j.ijpharm.2020.120141
41. Zhang B, Zhang Y, Dang W, et al. The anti-tumor and renoprotection study of E-[c(RGDfK)2]/folic acid co-modified nanostructured lipid carrier loaded with doxorubicin hydrochloride/salvianolic acid A. *J Nanobiotechnol*. 2022;20(1):425. doi:10.1186/s12951-022-01628-x
42. He C, Hu Y, Yin L, Tang C, Yin C. Effects of particle size and surface charge on cellular uptake and biodistribution of polymeric nanoparticles. *Biomaterials*. 2010;31(13):3657–3666. doi:10.1016/j.biomaterials.2010.01.065
43. Xiao K, Li Y, Luo J, et al. The effect of surface charge on in vivo biodistribution of PEG-oligocholic acid based micellar nanoparticles. *Biomaterials*. 2011;32(13):3435–3446. doi:10.1016/j.biomaterials.2011.01.021
44. Duan X, Li Y. Physicochemical characteristics of nanoparticles affect circulation, biodistribution, cellular internalization, and trafficking. *Small*. 2013;9(9–10):1521–1532. doi:10.1002/smll.201201390
45. Wu W, Luo L, Wang Y, et al. Endogenous pH-responsive nanoparticles with programmable size changes for targeted tumor therapy and imaging applications. *Theranostics*. 2018;8(11):3038–3058. doi:10.7150/thno.23459
46. Li C, Guan H, Li Z, Wang F, Wu J, Zhang B. Study on different particle sizes of DOX-loaded mixed micelles for cancer therapy. *Colloids Surf B Biointerfaces*. 2020;196:111303. doi:10.1016/j.colsurfb.2020.111303
47. Kebebe D, Wu Y, Zhang B, et al. Dimeric c(RGD) peptide conjugated nanostructured lipid carriers for efficient delivery of gambogic acid to breast cancer. *IJN*. 2019;14:6179–6195. doi:10.2147/IJN.S202424
48. Yan J, Chen J, Zhang N, et al. Mitochondria-targeted tetrahedral DNA nanostructures for doxorubicin delivery and enhancement of apoptosis. *J Mater Chem B*. 2020;8(3):492–503. doi:10.1039/C9TB02266J
49. Duan S, Zhang M, Li J, et al. Uterine metabolic disorder induced by silica nanoparticles: biodistribution and bioactivity revealed by labeling with FITC. *J Nanobiotechnol*. 2021;19(1):62. doi:10.1186/s12951-021-00810-x
50. Dong H, Diao H, Zhao Y, et al. Overexpression of matrix metalloproteinase-9 in breast cancer cell lines remarkably increases the cell malignancy largely via activation of transforming growth factor beta/SMAD signalling. *Cell Prolif*. 2019;52(5):e12633. doi:10.1111/cpr.12633
51. Padmanaban V, Krol I, Suhail Y, et al. E-cadherin is required for metastasis in multiple models of breast cancer. *Nature*. 2019;573(7774):439–444. doi:10.1038/s41586-019-1526-3
52. Kawiak A, Kostecka A. Regulation of Bcl-2 family proteins in estrogen receptor-positive breast cancer and their implications in endocrine therapy. *Cancers*. 2022;14(2):279. doi:10.3390/cancers14020279